Ad Hoc Networks 38 (2016) 38–50

Contents lists available at ScienceDirect

Ad Hoc Networks

journal homepage: www.elsevier.com/locate/adhoc

An adaptive wireless passive human detection via fine-grained physical layer information

Liangyi Gong[a], Wu Yang[a,*], Zimu Zhou[b], Dapeng Man[a], Haibin Cai[c], Xiancun Zhou[d], Zheng Yang[e]

[a] College of Computer Science and Technology, Harbin Engineering University, Heilongjiang Province, China
[b] Department of Computer Science and Engineering, Hong Kong University of Science and Technology, Hong Kong, China
[c] Software Engineering Institute, East China Normal University, China
[d] Department of Information Engineering, West Anhui University, China
[e] School of Software and TNList, Tsinghua University, Beijing, China

ARTICLE INFO

Article history:
Received 17 March 2015
Revised 14 September 2015
Accepted 15 September 2015
Available online 2 November 2015

Keywords:
Device-free passive
Human detection
PHY layer information
Multipath propagation

ABSTRACT

Wireless device-free passive human detection is a key enabler for a range of indoor location-based services such as asset security, emergency responses, privacy-preserving children and elderly monitoring, etc. Since the feature of received signal varies with different multipath propagation conditions, an labor-intensive on-site calibration procedure is almost indispensable to decide the optimal scenario-specific threshold for human detection. Such overhead, however, impedes readily and fast deployment of wireless device-free human detection systems in practical indoor environments. In this work, we explore PHY layer multipath profiling information to extract a novel quantitative metric K_s as an indicator for link sensitivity, and further exploit a linear detection threshold prediction model. We design an adaptive device-free human detection scheme that automatically predicts the detection threshold according to the richness of multipath propagation within monitored areas. We implement our scheme with commodity WiFi infrastructure and evaluate it in typical office environments. Extensive experimental results show that our scheme yields comparative performance with the state-of-the-art, yet requires no on-site threshold calibration.

1. Introduction

Indoor location-based service (LBS) is fast permeating into ordinary people's daily life due to convenience, production and recreation. The ability to perceive the presence of users within the area of interests by LBS providers is crucial to deliver numerous context-aware services such as navigation and location-based advertisements [1]. Recent advances in wireless technology and the pervasive deployment of wireless infrastructure have raised increasing research interests to leveraging the ubiquitous wireless signals to fulfill this task in a *device-free* manner [2]. In principle, wireless-based device-free human detection works by extracting and analyzing radio shadowing and reflection induced by human motions from wireless monitors deployed in advance, while the target users carry no wireless devices [3–6]. Such device-free human detection mode is especially advantageous in asset security, emergency responses, privacy-preserving elderly monitoring, etc.

A typical wireless device-free human detection system consists of one or multiple transmitter-receiver (TX-RX) links [4,7]. Each TX-RX link operates in two steps: on-site calibration and online monitoring. During the on-site calibration stage, a receiver measures and stores signal features when no one exists within a monitored area, and builds up

* Corresponding author. Tel.: +45182589638.
E-mail address: yangwu@hrbeu.edu.cn (W. Yang).

http://dx.doi.org/10.1016/j.adhoc.2015.09.005
1570-8705/

a *normal profile*. It also collects the signal features with human moving within the monitored area, and decides a detection threshold to distinguish the two cases. Afterwards the receiver turns into the online monitoring stage by comparing the measured signal features with the normal profile. Once the deviation from the normal profile exceeds or is below the pre-calibrated threshold, the receiver announces an abnormal event. Such calibration overhead significantly hampers the fast deployment of wireless human detection systems for a new environment, especially in indoor environments.

Although Received Signal Strength Indicator (RSSI)-basd passive human detection [5,8] explores to realize lightweight human detection, only by employing a single normal profile without calibration, it suffers serious performance degradation due to indoor multipath effect. In indoor environments, it is common for wireless signals to transmit to the receiver via multiple paths, which is called the multipath effect. Multipath fading can cause constructive or destructive interference. Different multipath superposition status can lead to diverse link behaviors in reaction to human motions [8] and varied detection coverage shapes [9]. For RSSI-based passive human detection, when a person disturbs a radio link, the RSSI of the link may decrease, increase, or even remain unchanged. Channel state information (CSI), as a fine-grained signal feature [10], characterizes the multipath effect at the granularity of OFDM subcarrier in the frequency domain [11]. It is employed for indoor passive human detection in a revolutionary way and shows good performance. However, existing CSI-base passive human detection systems [7,12,13] more rely on stationary signal patterns, and are *blind* to the propagation conditions where a TX-RX link is deployed and the sensitivity of receivers in dynamic states. The calibration overhead is indispensable if systems were to achieve optimal detection performance under a new multipath propagation environment.

In this work, we raise the question from a unique perspective: instead of blindly relying on on-site calibration or stationary signal patterns to determine the optimal threshold, can we predict the optimal threshold based on assessment of the current multipath propagation conditions without incurring dramatic performance degradation? The key insight is that the threshold to distinguish static and dynamic is closely related to the *sensitivity* of a TX-RX link to human motions. Based on extensive measurements, we observe that such difference in sensitivity to human motions is a result of different multipath propagation conditions. Thus given a quantitative characterization of the multipath propagation conditions, we may predict a threshold without calibration for a new environment. To achieve this goal, we need to address multiple challenges. (1) *How to derive a quantitative metric associated with sensitivity to human motions?* (2) *How to measure the sensitivity metric on commodity wireless devices?* (3) *How to predict the threshold for CSI-based passive human detection based on the sensitivity metric?*

To tackle these challenges, we leverage the recently exposed PHY layer Channel State Information (CSI) on standard IEEE 802.11a/g/n Network Interface Cards (NICs). We take a measurement-driven approach to extract from CSIs an indicator for link sensitivity to human motions. We demonstrate that the metric depicts the abundance of multipath propagation, and is directly measurable using CSI data sampled when there is no human in the area of interests. In addition, we put forward a novel decision model where the proposed metric is harnessed to predict the optimal threshold without on-site calibration for a new environment. To validate the effectiveness of our model, we implement a passive human detection system using off-the-shelf WiFi infrastructure. Extensive experiments conducted in two academic buildings show that the proposed metric can act as a proxy for link sensitivity levels. Compared with the state-of-the-art PHY layer CSI based human motion detection systems [7], our threshold prediction scheme achieves competitive detection performance, while requiring no cumbersome on-site threshold calibration.

Our main contributions are summarized as follows.

- We harness PHY layer frequency-diversity information on commodity WLAN infrastructure to characterize the richness of multipath propagation, and derive an innovative metric to quantitatively evaluate the link sensitivity to environment changes.
- We design an adaptive passive human detection scheme that automatically predicts the detection threshold according to the richness of multipath propagation within a monitored area. It relies on not only stationary signal patterns but also receiver sensitivities in dynamic states. It requires minimal calibration efforts while retaining high detection rates and is helpful to fast deployment of detection systems and avoid frequent system re-calibrations.
- We prototype our scheme on off-the-shelf WiFi devices. Extensive evaluations in typical office environments demonstrate that compared with the state-of-the-art, our scheme achieves comparable detection performance even without on-site calibration for a new environment, which enables fast and lightweight deployment of wireless device-free intruder detection systems in practical indoor environments.

In the remaining of this paper, we provide a preliminary in Section 2, followed by measurements on detection sensitivity in Section 3. We detail the threshold prediction scheme in Section 4.2, and present the performance evaluation in Section 5, followed by brief discussions in Section 6. Section 7 reviews the related work, and Section 8 concludes this work.

2. Preliminary

Wireless passive human detection identifies a person by analyzing the impact of human motions on received signals, while the intruder does not carry any wireless-enabled device [3]. Such motion-induced impact usually leads to dramatic changes in certain received signal features, where Received Signal Strength Indicator (RSSI) acts as the most prevalent signal feature due to its easy access [3,4,14–16]. Recent advances in wireless techniques have also raised increasing interest in utilizing the PHY layer Channel State Information (CSI) on commodity WiFi NICs for finer-grained human motion detection [7,17]. In this section, we review the general framework of wireless passive intruder detection systems, and point out the challenges for fast deployment in practical multipath-dense environments. Then We provide a brief introduction on CSI. Finally, we expound a specific CSI-based human detection scheme with calibration.

2.1. Wireless passive human detection

Most of wireless passive human detection system work in two steps: on-site calibration and online monitoring. In the on-site calibration stage, a receiver collects the signal features when there is no intruder within the area of interests, and builds up a *normal profile* as a reference. Then it measures the signal features with intruders moving within a monitored area, and decides an optimal threshold to distinguish the two cases. After choosing the optimal threshold under certain accuracy constraints, the receiver switches to online monitoring mode, and compares the measured features. Once the signal feature exceeds the pre-calibrated threshold, the receiver announces an abnormal event. The on-site calibration stage, however, requires a professional user to traverse the monitored area so that the receiver can collect sufficient and comprehensive measurements to determine an optimal threshold, and is often scenario-specific. That is, re-calibration is usually necessary to maintain satisfactory detection performance in case of environmental dynamics such as the removal of a piece of furniture, or the locations changes of TX-RX links.

While numerous efforts have explored to derive close-form models of human-induced impact on received signals [9,18,19], dense multipath propagation indoors often deteriorates the effectiveness of these models, thus leading to irregular detection ranges [9,20] and unreliable detection results [8]. Consequently, the on-site calibration stage is almost indispensable and usually scenario-specific, since the multipath propagation tends to vary with environments. Hence a threshold for one scenario can lead to substantial performance degradation in another monitoring area without re-calibration. Such site-specific calibration efforts incur cumbersome overhead, thus impeding fast deployment of wireless human detection systems in practical multipath-rich indoor environments.

A primary reason for such re-calibration overhead is that existing schemes are often blind to the multipath propagation conditions where the monitors are deployed. While conventional RSSI fails to depict multipath propagation conditions, the PHY layer CSI provides finer-grained channel measurements.

2.2. Channel state information

The MAC layer RSSI serves as a prevalent indicator for channel quality, yet is a superposition of multipath signals. To resolve multipath propagation at a finer granularity, pioneer work has explored PHY layer Channel State Information (CSI) [11]. Each CSI depicts the amplitude and phase of an OFDM subcarrier:

$$H(f_k) = \|H(f_k)\| e^{j\angle H(f_k)} \tag{1}$$

where $H(f_k)$ is the CSI at the subcarrier with frequency of f_k, and $\angle H(f_k)$ denotes the corresponding phase [21].

Compared with the MAC layer RSSI, CSI distinguishes multipath components at subcarrier level [22]. In the subsequent sections, we derive measurable metrics from CSI as indicator for link sensitivity, and further utilize the metric to predict the threshold for human detection.

2.3. CSI-based human detection via calibration

Since human motions tend to induce temporal fluctuations in the received signals, it is natural to employ temporal correlation of CSIs as a metric to calculate the deviations of CSIs from a normal profile. The normal profile is considered as a basis signal features set. In order to construct a normal profile, we generally collect n packets at different times of day when there is no one within the monitored area and pick m packets at random for eliminating noise effects. The corresponding CSIs can be extracted and stored as the normal profile H_{nor}:

$$H_{nor} = [H^1_{nor}, H^2_{nor}, \cdots, H^m_{nor}] \tag{2}$$

where each H^k_{nor} is the CSI amplitudes of the k^{th} selected packet in the normal profile.

Different from RSSI, as a fine-grained signal feature, the CSIs of single TX-RX pair can be employed to detect the human motion in non-line-of-sight paths. As shown in Fig. 1a, when a person walks around in the indoor area of interest, there is no clear a gap between kernel density of abnormal state and that of normal state. In order to determine the optimal detection threshold, we need to collect the CSIs information in static and dynamic scenarios. Hence, we firstly collect a total of about 10 min of N packets without human motion and then extract the CSI amplitudes. Denote the CSI amplitudes of the i^{th} packet as H^i_{sta}. Then we calculate its average cross-correlation with the CSI amplitudes of the normal profile:

$$C^i_{sta} = \frac{1}{m}\sum_{k=1}^{m} corr(H^i_{sta}, H^k_{nor}) \tag{3}$$

And we denote $C_{sta} = \{C^i_{sta}\}^N_{i=1}$ as the set of cross-correlation values without human motion.

Similarly, we collect another N packets with one person walking around within the monitored area, and calculate the corresponding average cross-correlation values with the normal profiles:

$$C^i_{dyn} = \frac{1}{m}\sum_{k=1}^{m} corr(H^i_{dyn}, H^k_{nor}) \tag{4}$$

And we denote $C_{dyn} = \{C^i_{dyn}\}^N_{i=1}$ as the set of cross-correlation values with intruders.

Although the probability density distributions of the cross-correlation values exhibit an unconspicuous shift with and without human motion, we can also distinguish the two cases with some pre-defined accuracy requirements. More specifically, given the Cumulative Distribution Functions (CDFs) of the cross-correlation values $F(C_{sta})$ and $F'(C_{dyn})$, as in Fig. 1(b), the optimal detection threshold C is determined by:

$$C = F'^{-1}(\beta) = F^{-1}(\alpha) \tag{5}$$

where $\alpha \in (0, 1)$ and $\beta \in (0, 1)$. They are cumulative distribution values of cross-correlation in static and dynamic cases, respectively. In most cases, we need to set either α or β. The upper bound of abnormal case is equal to the percentile of the CDF function $F'(C_{dyn})$, such that $C^{max}_{dyn} = F'^{-1}(\beta)$. The low bound of normal case is equal to the percentile of the CDF function $F(C_{sta})$, such that $C^{min}_{sta} = F^{-1}(\alpha)$.

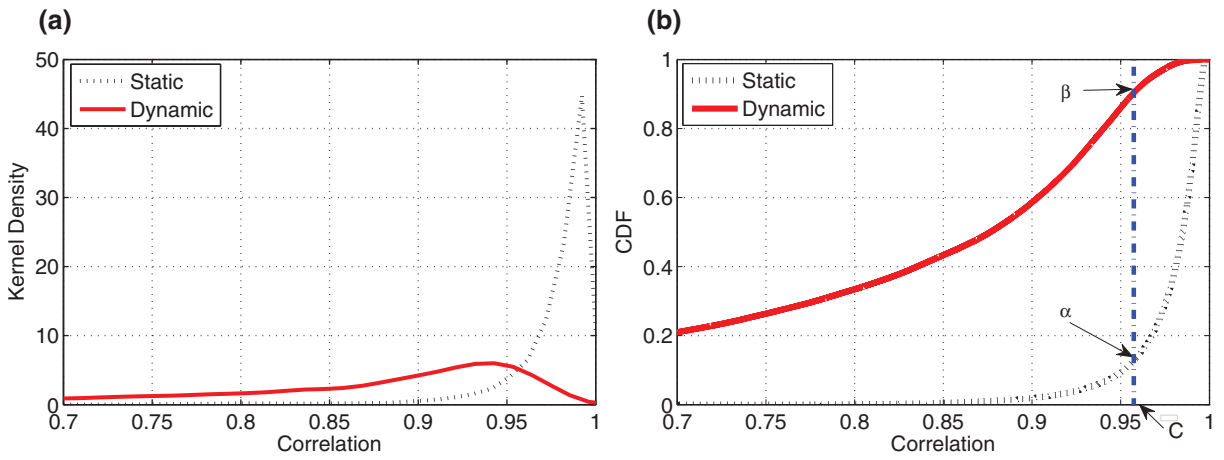

Fig. 1. Distributions of cross-correlation and illustration of threshold determination.

The evaluation metrics for human detection system are mainly focused on the following metrics: (1) False Negative (FN): the fraction of cases where the receiver fails to detect human motion within the monitored area. (2) False Positive (FP): the fraction of cases where the receiver announces human motions when there is no one around. $F^{-1}(\alpha)$ and $F'^{-1}(\beta)$ depict the requirements on false positives and false negatives for the detection system. The larger α or β can cause higher FP and lower FN, and the less α or β can cause lower FP and higher FN. Hence, the selection of α or β provides a tradeoff between FN and FP.

In order to reduce the calibration efforts, some systems [5,23] realize light-weight passive human motion detection based on a normal profile. When the significance α is pre-set, the detection threshold can be readily calibrated by $C = F^{-1}(\alpha)$. However, the indoor multipath propagation condition of signals is often ignored. In different indoor scenarios, the receiver signal performs various reactions to human motion. In the same indoor scenarios, when the receiver is placed at different locations, the receiver even owns different link sensitivities. The optimal detection threshold C related to the α changes with different link sensitivity. In the following section, we detail the influence of link sensitivity on the selection of significance α.

3. Link sensitivity

As previously discussed, different multipath propagation conditions may lead to different sensitivities to human motions, which further affects the threshold for human detection. In this section, we demonstrate link sensitivity and its impact on the detection threshold in detail.

3.1. Multipath propagation vs. link sensitivity

In multipath-rich indoor environments, wireless signals can be transmitted to a receiver via reflection, diffraction and scattering [24], and human motions tend to alter signal propagation in a more sophisticated manner, thus leading to different sensitivity levels at a receiver. Assuming evenly distributed reflectors or scatters, the sensitivity region can be characterized by an ellipse along the TX-RX link [9]. While a person starts to move towards the LOS path, he would induce notable shadowing and create additional reflections which can be observed by a receiver [19]. For different receiver locations, these multipath components can superpose either constructively or destructively [8], and the ratio of the NLOS paths in the total received signals also varies. With large amount of NLOS paths, human motions are likely to disturb more paths, thus resulting in more severe fluctuations of the received signals. In contrast, with only a strong LOS path, human motions can only significantly affect the received signals in close proximity to the LOS path. As a result, human motions tend to induce less notable changes of the received signals. Therefore, the sensitivity level of the receiver is closely related to the richness of the NLOS paths in the received signals.

3.2. Impact of link sensitivity

Note that the threshold is determined by the difference between the CDFs of the cross-correlation values with and without human. In this subsection, we demonstrate through measurements that the CDFs of these cross-correlation values vary with different link sensitivities to human motions.

As a preliminary test, we place a TX-RX link as shown in Fig. 2, and a user walks back and forth out of the First Fresnel zone of the link. We record the corresponding CSIs collected at RX1 and RX2 in Fig. 3. As shown in Fig. 3(a), the CSIs received at RX1 only suffer slight changes when the user moves, yet experience notable fluctuations at RX2 (Fig. 3(b)). Hence receivers at different locations can exhibit different sensitivity levels to the same human motions.

Such different receiver sensitivities also affect the CDFs of the cross-correlation features. As shown in Fig. 4, the CDFs of the cross-correlation features distribute more narrowly under low sensitivity, yet span a wider range in case of high sensitivity. Consequently, the optimal threshold to detect human motion also tends to differ. The detection threshold when the receiver possesses high sensitivity is about 0.96, but that with low sensitivity is about 0.94. The α with hight sensitivity is about 0.2, but that with low sensitivity is about 0.3. It

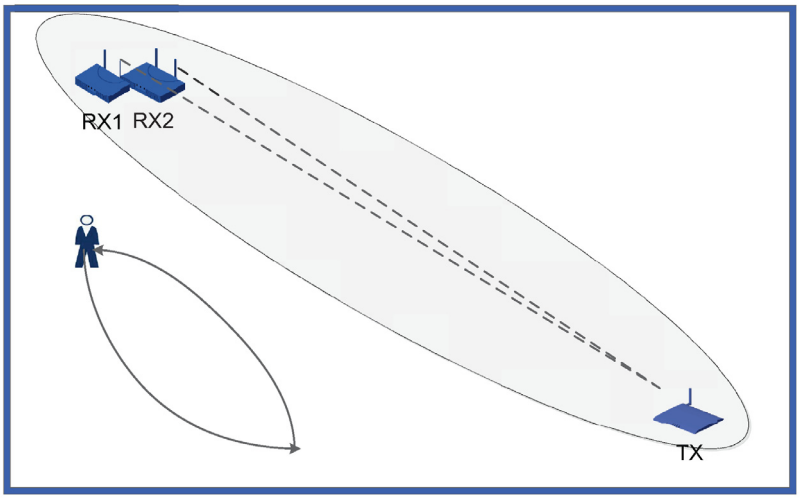

Fig. 2. Measurement Setup for Link Sensitivity.

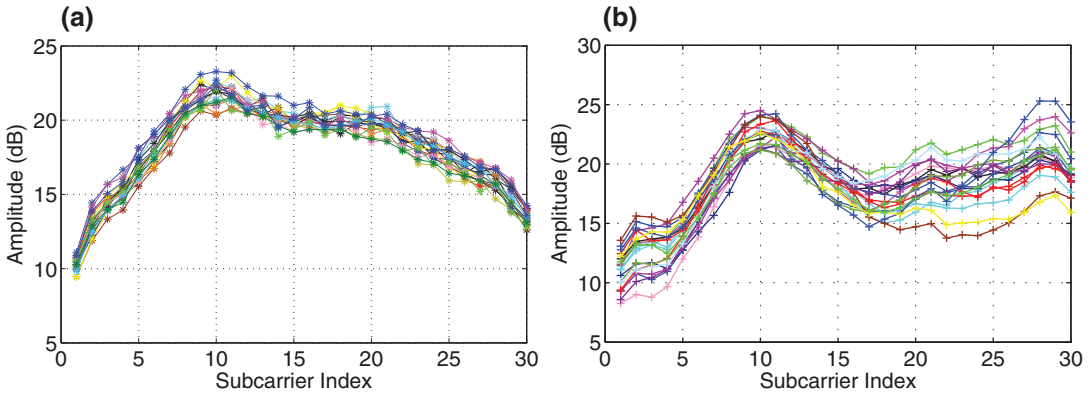

Fig. 3. Fluctuations of CSI Amplitudes Under Different Sensitivity.

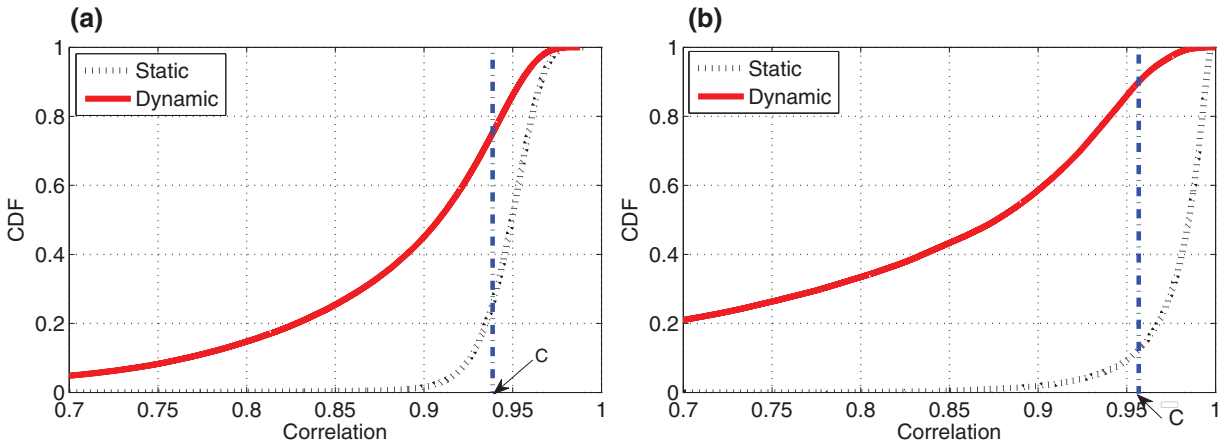

Fig. 4. CDFs of Cross-correlations Under Different Sensitivity.

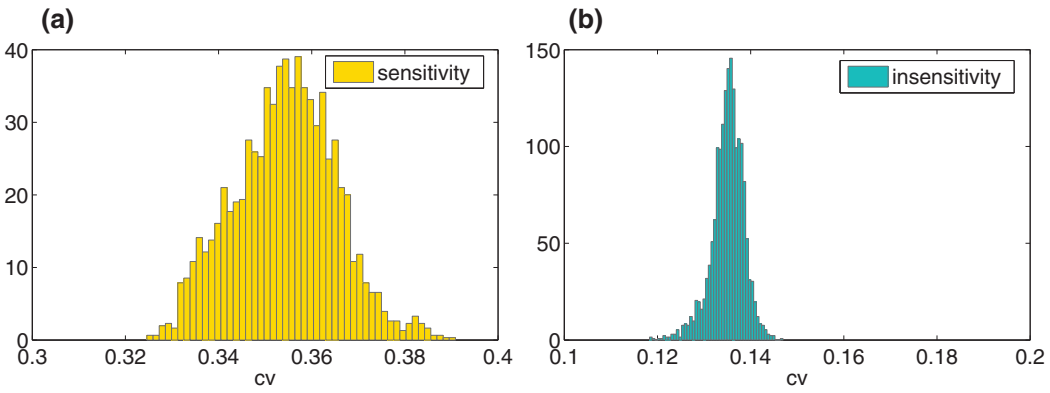

Fig. 5. Distributions of the *cv* Values Under Different Sensitivity.

is thus possible for one threshold calibrated at one link deployment to result in significant performance degradation at another link layout due to different sensitivity levels. In the subsequent sections, we elaborate how to quantify the sensitivity levels and strive to extract a measurable indicator for different sensitivity levels without on-site calibration.

4. Adaptive passive human detection

4.1. The K_s metric

In communications communities, Rician *K* factor is defined as the power ratio of the LOS to the NLOS paths to indicate the richness of multipath propagation [24]. Theoretically, if the received envelope *r* follows Rician distribution, then it can be depicted by Rician *K* factor *K* as follows [25]:

$$p(r) = \frac{2(K+1)r}{\Omega} e^{(-K-\frac{(K+1)r^2}{\Omega})} I_0\left(2r\sqrt{\frac{K(K+1)}{\Omega}}\right) \tag{6}$$

where $I_0(\cdot)$ is the zero order modified Bessel function of the first kind, and Ω denotes the total received power. A practical estimator for Rician *K* factor [25] is as follows:

$$\hat{K} = \frac{-2\hat{\mu_2^2} + \hat{\mu_4} - \hat{\mu_2}\sqrt{2\hat{\mu_2^2} - \hat{\mu_4}}}{\hat{\mu_2^2} - \hat{\mu_4}} \tag{7}$$

where $\hat{\mu_2}$ and $\hat{\mu_4}$ are the empirical second and fourth order moments of the measured data, respectively. While Rican *K* factor has been adopted in applications such as LOS identification [26], it becomes insensitive to the changes of multipath components in case of a weak LOS path [27]. To improve the performance of Rician *K* factor in NLOS dominant scenarios, some research exploits the forth-order moments of received phase as a metric to assess the abundance of multipath propagation [27]. Nevertheless, due to lack of time and phase synchronization, it is often difficult to extract accurate phase information on commodity WiFi devices [28,29].

Towards a lightweight indicator for multipath propagation, we resort to the statistical features of CSI amplitudes available on commercial WiFi infrastructure. The reasons for utilizing CSI to characterize the abundance of multipath propagation are two-fold:

- The received power transmitting through the NLOS paths is significantly affected by the reflectors and scatters along the paths [7,23].
- The attenuation caused by shadowing, reflection and scattering relates to frequency. In general, signals with higher frequency suffer more severe attenuation when penetrating obstacles [30].

Since the spectrum of OFDM signals is relatively flat, we can assume that the transmission power on each subcarrier is almost the same. Therefore, in case of only a strong LOS path, signals transmitting on each subcarrier would propagate through the same path and thus the received power of each subcarrier remains similar if normalized to the same frequency. In contrast, in case of rich NLOS propagation, signals with higher frequencies might be too severely attenuated to be detected by the receiver. Therefore the received signal powers may deviate from each other even when normalized to the same frequency. Leveraging such frequency-selective fading, we may be able to assess the abundance of multipath propagation, as well as the sensitivity level of receivers.

As a primary verification, we collect CSIs under both low and high sensitivity levels. We then normalize the CSI amplitude of each subcarrier to the central carrier frequency f_0 as follows:

$$H_{norm}(f_k) = \frac{f_k}{f_0} \cdot H(f_k) \tag{8}$$

where $H(f_k)$ and $H_{norm}(f_k)$ are the original and normalized (w.r.t. f_0) amplitudes of the k^{th} subcarrier. f_k is the frequency of the k^{th} subcarrier. To further eliminate the impact of measurement scales and obtain a dimensionless quantity, we calculate the coefficient of variation of the normalized CSI amplitudes as follows:

$$cv = \frac{std(H_{norm})}{mean(H_{norm})} \tag{9}$$

where $std(H_{norm})$ and $mean(H_{norm})$ are the standard deviation and mean of the normalized CSI amplitudes H_{norm}, respectively. Fig. 5 plots the distributions of the coefficients of variation. As is shown, *cv* values under low sensitivity are smaller and distribute within a narrow range, while those under high sensitivity are larger and span a wider range. To quantify the

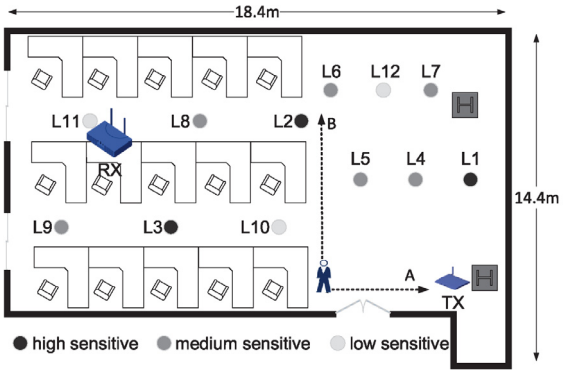

Fig. 6. Measurement Setup of K_s.

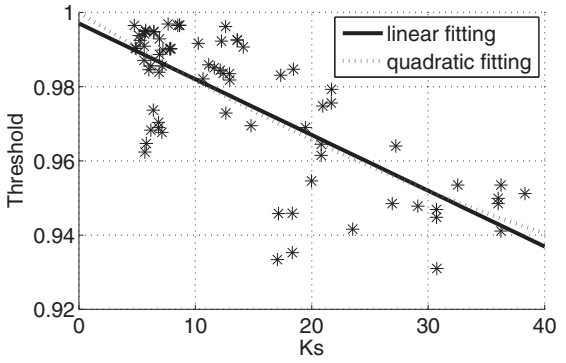

Fig. 7. Threshold Prediction Using K_s.

Table 1
K_s value and Rician K factor vs. sensitivity.

RX Location	K_s	K factor	Sensitivity
L1	3.89	641.44	High
L2	3.96	31.80	High
L3	4.37	317.36	High
L4	5.01	250.16	Medium
L5	5.54	285.27	Medium
L6	6.67	652.63	Medium
L7	7.27	222.33	Medium
L8	8.27	146.29	Medium
L9	9.26	283.15	Medium
L10	13.15	506.84	Low
L11	18.29	285.70	Low
L12	27.41	421.21	Low

difference among cv distributions, we employ a new metric K_s as follows:

$$K_s = \frac{\frac{E\{x-\mu\}^4}{\sigma^4}}{\mu} \tag{10}$$

where x, μ and σ denote the measurement, mean, and standard deviation of the cv values, respectively. As shown in Eq. 10, the more peaked the distribution of cv values, the larger K_s. And the larger the mean of cv values, the larger K_s.

To validate the effectiveness of Eq. 10, we conduct the following measurements. As shown in Fig. 6, we fix the location of the transmitter, and place a receiver at different locations. For each receiver location, we let a person walk within A and B, and collect 6000 data packets. We also collect the same amount of packets when there is no person in the monitored area. By calculating and comparing the CDFs of the cross-correlations with and without intruders as in Section 3.2, we rank the sensitivity of these receiver locations into three levels and mark the sensitivity levels in Fig. 6. As is shown, at different receiver locations, since the richness of multipath propagation differs, the sensitivity level to human motions also varies. We then calculate K_s values for each receiver location using data collected when there is no person in the monitored area. We also calculate Rician K factors using the same measurements. Table 1 lists K_s values, Rician K factors, and the corresponding sensitivity levels for each tested receiver locations. As is shown, K_s values roughly increase monotonously with the decrease of sensitivity levels at each receiver location. In contrast, no notable trend can be seen between Rician K factors and sensitivity levels. We thus employ K_s value as an indicator for the multipath propagation conditions, which further quantify sensitivity level of a receiver in some location.

4.2. Threshold prediction

As discussed in Section 3, when the location of a receiver changes, the detection sensitivity to human motions also changes due to different multipath propagation conditions. Therefore re-calibration is often indispensable if the human detection system is deployed in another environment to decide a new threshold, which is time-consuming and labor-intensive. Moreover, environmental dynamics such as the removal of a piece of furniture and slight location changes of the transmitter or the receiver may also lead to significant change of the optimal threshold. In this section, we explore to predict a decision threshold by assessing the current multipath propagation conditions, thus eliminating the need for frequent re-calibration without incurring dramatic detection performance degradation.

As we have demonstrated in Section 4.1, K_s serves as an indicator for the richness of multipath propagation. Since the K_s value is directly measurable from the normal profile, we hence explore to utilize K_s to predict the threshold for human detection. We conduct a measurement campaign in two academic buildings and collect 76 groups of data. Each test is conducted in a similar procedure as in Section 3.2. After collecting CSIs for the cases with and without human, we calculate the optimal threshold that may differ for specific application scenarios. Hence we explore the relationship between K_s and C. Fig. 7 plots the relationship between K_s and the envisioned threshold C. We also plot the linear and quadratic fitting results between K_s and C. As is shown, the threshold roughly falls linearly with the increase of K_s, that is $C = a * K_s + b$.

Factor K_s and detecting threshold are approximately linear, yet the coefficients (a, b) of fitting equations are not globally invariable and influenced by several device-related factors including emitting power, antenna gain of transmitters and receivers, etc. As a result, for a pair of transmitter and receiver, a pre-calibrated empirical measurement is necessary to configure them and determine their coefficients only once before deploying the same type of devices to various scenarios, where the threshold will be automatically

Table 2
Comparison with the state of the art techniques.

Technique	Feature granularity	Cost	Sensing coverage	Detection performance
RASID	Coarse-grained	Small	Narrow	High FN, high FP
FIMD	Fine-grained	Large	Wide	Middle FN, low FP
Adaptive detection	Fine-grained	Small	Wide	Low FN, middle FP

calculated based on the known equation coefficients and the current K_s.

Intuitively, the larger K_s is, the less sensitive a receiver is to human motions. Therefore, it seems that a larger threshold is required to distinguish the cases with and without intruders. Nevertheless, the monotonously decreasing relationship between K_s and the threshold is actually more rational for the following reasons:

- Due to the complex interior structure, multipath signals tend to arrive at the receiver in clusters [31]. Hence the cross-correlations of the received CSI amplitudes may distribute discretely rather than evenly within a certain range.
- At low sensitivity levels, the receiver cannot detect human motions faraway from the LOS path. Yet when a person walks in the close vicinity of the LOS path, cross-correlation values would experience a sharp change. This is because low sensitivity levels correspond to the case of a strong LOS path along a wireless link. Hence only when a person walks near the LOS path can he alter abundant NLOS paths to induce notable fluctuations of the received signals. Therefore only a small threshold is sufficient to distinguish the substantial disturbance induced by human motions from the normal profile.
- At high sensitivity levels, a receiver can detect human motions presenting relatively faraway. In this case, the power of the LOS path only takes up a small portion in the total received power. Thus the impact of human motions on the received signals mainly comes from changes in the NLOS paths. Since human motions faraway affect fewer NLOS paths, the threshold to discern the intruder from the normal profile is relatively larger.

Note that sensitivity in our work refers to the ability to detect human motions on the NLOS paths, rather than those along or close to the LOS path. For receiver sensitivity with human motions along the LOS path, the changes in the received signals are mainly due to body shadowing. We leave the assessments of such receiver sensitivity to future work.

5. Evaluation

The previous sections present how to measure the multipath propagation conditions via K_s value from the PHY layer CSI data, and further predict the decision threshold using metric K_s. In this section, we present the detailed evaluations on how well such predicted threshold perform in wireless device-free intruder detection. We first interpret the experiment methodology, followed by detailed performance evaluation results in typical office environments including multipath-dense scenarios and NLOS propagation.

5.1. Methodology

Testing Scenarios: We conduct the measurement campaign in three typical indoor scenarios in two academic buildings. Each testing room is occupied with desks, chairs, and other furniture, so as to create different extent of multipath propagation. To mitigate the impact of particular room structures, we test two symmetric TX-RX pairs for each scenario (TX1-RX1 and TX2-RX2 in Figure 8). We detail each testing scenario as follows:

- **Scenario 1:** A 12.4 m $\times$ 7.2 m classroom furnished with rows of desks and chairs. TX and RX are placed 10 m away and 1.5 m in height (Fig. 8(a)).
- **Scenario 2:** A 7.2 m $\times$ 6.4 m office room with cubic desks, chairs, computers and other plastic and metal furniture. TX and RX are placed 7m away and 1.2m above the floor (Fig. 8(b)).
- **Scenario 3:** A meeting room of 5.6 m $\times$ 4.2 m equipped with a rectangular conference table and several chairs. TX and RX are placed 5m away and about 1.1 m above the floor (Fig. 8(c)).

Infrastructure Setup: We employ a single-antenna Tenda W3000R wireless router as the TX operating in IEEE 802.11n AP mode at 2.4GHz. A LENOVO Thinkpad X200 laptop equipped with Intel 5300 NIC and 2 antennas running Ubuntu 10.04LTS server OS works as the RX pining packets from the TX. The two antennas are 6cm away from each other (approximately half wavelength of the 2.4 GHz WiFi signals). The firmware is modified as [11] to extract CSIs from data packets using the CSI tool [11].

Data Collection: For each scenario, we first need to find receiver locations with high and low sensitivities. We achieve this by fixing the transmitter, and slightly adjusting the location of the receiver and monitoring the fluctuations of CSI amplitudes using the *CSI Show tool* we developed as discussed in Section 4.1. For each TX-RX link setting as in Fig. 8, we choose three receiver locations with high sensitivity and 3 with low sensitivity. We then block the LOS path along the link and choose another 3 receiver locations with high sensitivity and 3 with low sensitivity, respectively. Thus in total we collect data for 12 receiver locations for each link pair. After choosing each receiver location, we collect CSI data using the CSI tool. The transmitter is configured to send ICMP packets at the rate of 20 Hz. For each receiver location, we collect 5000 packets with no intruder in the room to build up the normal profile and 2400 packets as test samples for the normal case. To collect test samples for the human motion case, we let a volunteer walk randomly in the room for 2 min. We recruit three volunteers in total and collect three groups of test samples for the human motion case at each receiver location.

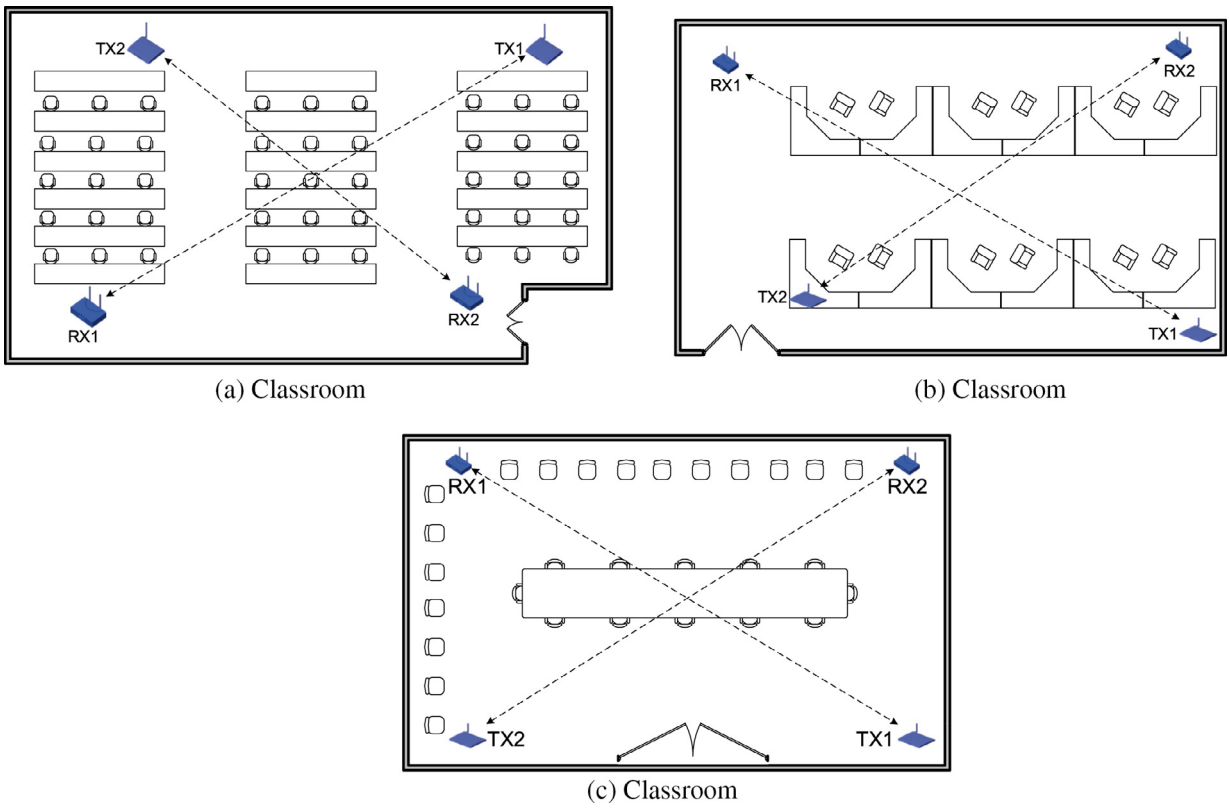

Fig. 8. Illustration of Testing Scenarios and Link Deployment in Two Academic Buildings.

5.2. Performance

5.2.1. Accuracy of threshold prediction

Since the threshold directly determines the detection performance (i.e. FN and FP), we evaluate the accuracy of our threshold prediction scheme as follows. We implement the state-of-the-art device-free passive human motion systems, RASID-like [5] and FIMD [7]. And we feed a large amount of training data to derive a threshold with balanced FN and FP performance as the optimal threshold. Then we only use the data without human motions to predict a threshold as detailed in Section 4.2. To compare the accuracy of the predicted threshold, we compare the detection performance using the optimal and the predicted thresholds in the three testing scenarios. Fig. 9 plots the FNs and FPs using the optimal and the predicted thresholds. As expected, due to the shortcoming of RSS and indoor multipath effect, RASID-like shows poor performance for human detection in the whole area of interest. Although FIMD outperforms RASID-like, it needs to select too many packets via caliberation, which is a challenge to human motion. In contrast, with the predicted threshold, our scheme still achieves an average FN of 3.72% with the corresponding FP of 3.61%. The performance loss may be less. Notably, our adaptive detection can eliminate the labor-intensive on-site calibration to determine the optimal threshold at the cost of only marginal detection performance degradation.

5.2.2. Performance under LOS/NLOS propagation

While many human detection systems are deployed with a LOS path along a TX-RX link [32], it is possible for the LOS path to be obstructed by furniture or irregular room structure. We thus evaluate our threshold prediction scheme in the scenarios with and without the presence of a strong LOS path along the TX-RX link (by using a metal broad to manually block the LOS path). As illustrated in Fig. 10, the average FN reaches 4.15% with a clear LOS path along the TX-RX link, and drops to 3.23% without the presence of the LOS path. In contrast, the average FP in case of a clear LOS path is 1.3% lower than that without the presence of a LOS path. This is partially because receiver locations with a strong LOS path, only human motions in the vicinity of the LOS path can be detected. The normal profiles are more stable with a strong LOS path, thus contributing to lower average FP rates. Simultaneously, when the LOS path is severely attenuated, the power of other multipath components would take up a large portion of the total received power, and thus contributing to higher sensitivity to environmental slight changes, even environmental noise.

5.2.3. Factor to improve the scheme

Further, We evaluate factors to improve the accuracy of our threshold prediction scheme, including package quantity and subcarrier number.

(1)package quantity: Since the calculation of K_s involves high-order statistics such as kurtosis, the amount of data can

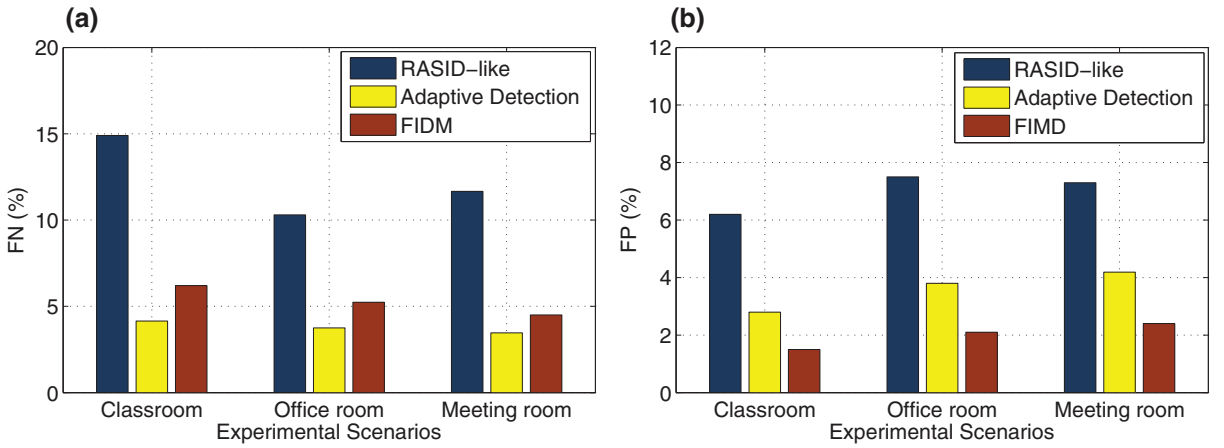

Fig. 9. Overall Motion Detection Performance in Different Scenarios.

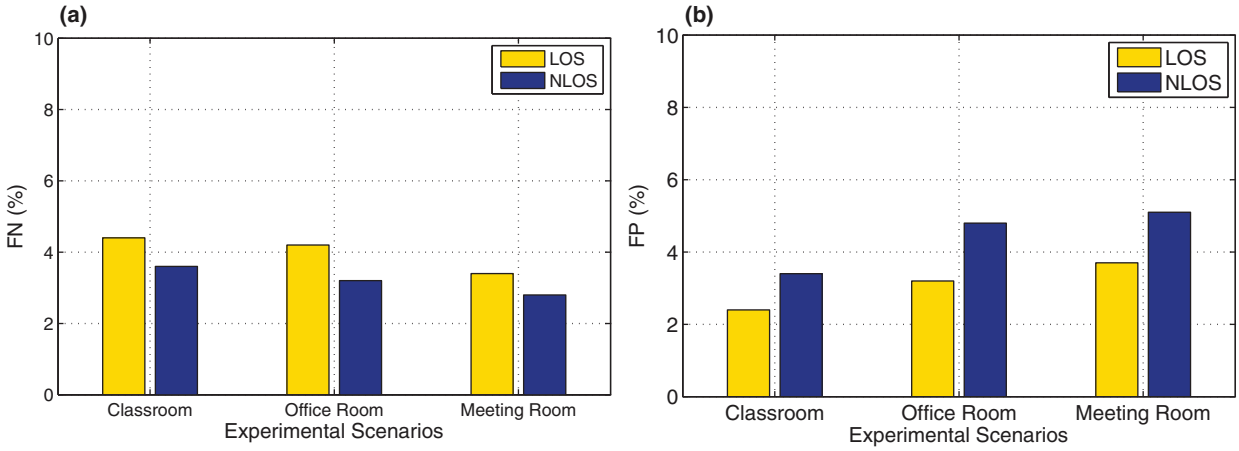

Fig. 10. Performance With and Without A LOS Path.

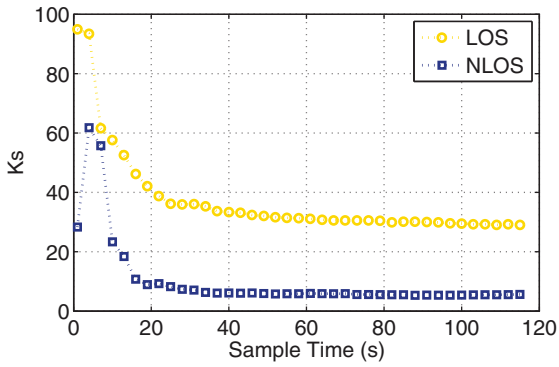

Fig. 11. Impact of Packet Quantity on the Estimation of K_s.

affect the accuracy of K_s estimation. We plot K_s estimation with different amount of packets under both LOS and NLOS propagation in Fig. 11. As is shown, a packet pinging rate below 20 packets per second will lead to an unstable evaluation while a packet pinging rate above 40 will stabilize. We advise to take 50 to get a good balance between accuracy and power consumption.

(2)subcarrier number: Compared with RSSI, CSIs of all subcarriers are fine-grained features. The number of subcarriers can have the effect on the performance of the scheme, including receiver sensitivity estimation, false negative and false positive.

As mentioned in Section 4.1, different subcarriers suffer from varying degrees of fading. The sensitivity estimation accuracy will be improved if more subcarriers are deployed. We evaluate the effect of subcarrier number, and figure out that the relationship between number of subcarriers and sensitivity estimating accuracy is closely linear when the number is below 35. Fig. 12 shows that the sensitivity estimation accuracy is raised as the number of subcarrier increases. When we employ 30 subcarriers, the accuracy of receiver sensitivity estimation can achieve about 90%.

6. Discussion and limitation

A. The power of low and high sensitivity

Factor K_s, as a metric of the sensitivity of received signals w.r.t. environmental dynamics, can be used not only for passive human detection, but also for wireless indoor localization. Pre-existing passive human detection systems are

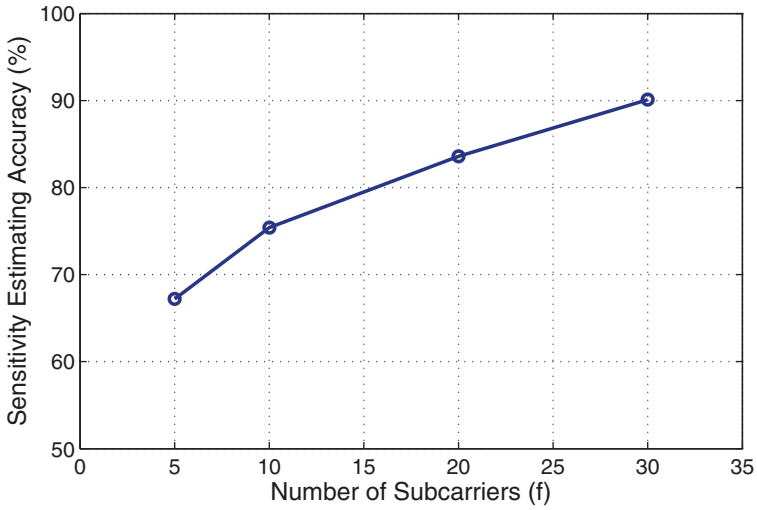

Fig. 12. Effect of Subcarrier Number on Sensitivity Estimation.

mostly based on the human body shadowing or reflection effect. For multi-link-based passive human detection on shadowing effect like [14,32], the alarms is better to occur when the human shadows or is close to the LOS path. Hence, sensing devices are preferred to deploy at positions with low sensitivity to combat multipath signal fluctuation caused by the human motion far from the LOS path. In contrast, for single-link-based passive human detection based on reflection effect like [12,13], the positions with high receiver sensitivity will be chosen to enhance the detecting rate and range, where the system successes in detecting subtle signal fluctuation caused by the human motion in NLOS paths. In addition, affected by different human body postures, the CSI collected at the same position is not constant [13]. Hence, for fingerprinting-based localization like [17,22,29], it is better to collect signal characteristics at some positions with a low receiver sensitivity, or equivalently, factor K_s is large. In this situation, the collected signal fingerprints are relatively stable and less effected by environment noise or human postures, etc, while the localization deviation will be accordingly reduced. In summary, multipath propagation is inevitable in indoor environment and we believe factor K_s is the key to take advantages of both high and low sensitivities.

B. Sensing coverage

Although the sensing coverage is extended to NLOS paths in this work, we do not specify the size or shape of sensible areas. The reasons lies in that the sensing coverage highly depends on complicated environmental factors, such as room layout, furniture, etc. In our experiments, the largest single room is about 90 m^2, which is typically a large indoor space in normal office buildings. It is a good choice to employ multiple TX-RX links for similarly even larger rooms. In our future work, we will study the effectiveness of K_s and the optimal deployment of multiple TX-RX pairs for accurate detection in large indoor spaces.

C. Qualitative comprehensive comparison

In Section 5.2.1, we make a quantitative comparison on the detection performance among different schemes, which demonstrates the high-efficiency of our scheme. In order to justify the effectiveness and advantage of our scheme, we further make a qualitative comprehensive analysis from four aspects: (1) **feature granularity**: our work and FIDM employ the fine-grained CSI with 30 subcarriers amplitudes as a base signal feature. The CSI is superior to RSSI(a single power value) and effective for depicting multi-path propagation and detect the NLOS human motion. (2) **cost**: our work and RASID achieve the passive human detection by leveraging only a normal profile collected in a few minutes, which is considered as a light-weight detection technique. But FIMD needs to learn predefined threshold and collect too many packets, which is a challenge to detection [13]. (3) **sensing coverage**: due to the fine-grained features of CSI, our work and FIMD can detect a person in a wide sensing coverage. The radius of sensing coverage can be up to 2 $\sim$ 3m, but the radius of sensing coverage of RSSI-based schemes is less than 1 m [13]. If the receiver is placed in the positions with small K_s factor, the radius of sensing coverage of CSI-based detection can be further improved. 4) **performance**: Our work and FIMD employ the temporally stable CSI and effectively reduce the FN and FP. For the NLOS human detection [12,13], the FN of CSI-based schemes including our work mostly is less than 5%, but the FN of RSSI-based schemes is more than 5%. Through the above analysis, we can observe that our work performances better among different aspects. Therefore, we agree that our work can be considered as a fine-grained, low-cost, high-efficient passive human motion detection with low system complexity.

7. Related work

Our work is closely related to the following researches.

Device-free passive (DfP) systems detect, locate, and track an intruder who carries no wireless devices via his impact on wireless signals received on wireless devices already deployed in the environments [3]. The underlying wireless infrastructure varies, including ZigBee nodes [15], WiFi transceivers [3,5], RFID tags [16,33], etc. Most systems utilize the MAC layer RSSI as signal features due to its easy

access. Nevertheless, RSSI can fluctuate dramatically even at a stationary link [22], thus leading to unreliable detection results. To compensate for the unreliable detection of RSSI, researchers resort to a dense deployment of wireless sensor networks to image human motions via Radio Tomographic Imaging (RTI) techniques [14,32]. In this work, we explore to measure the detection sensitivity of a single wireless link, and we envision that our work can provide guidelines for deploying the wireless monitors for better coverage and higher detection rates.

CSI depicts multipath propagation at the granularity of OFDM subcarriers and is accessible on commodity WiFi devices with minimal firmware modifications [11]. The finer-grained channel information has triggered an increasing research interest in PHY assisted indoor localization including accurate ranging [22] and fingerprinting [29]. CSI has also been employed for device-free human motion detection [7,13,17]. Zhou [17] proposed an omnidirectional passive human detection system through utilizing PHY layer fingerprinting features to virtually tune the shape of monitoring coverage. PADS [12] extracted available phase information of WLAN CSIs and combined the amplitude with the phase to realize the real-time human moving detection based on precalibration. In [13], authors proposed a Behavior-free passive motion detection system that monitors the moving human based on a normal profile. Our work is also built upon the CSI-based device-free detection framework. Yet unlike existing schemes that require on-site and scenario-specific threshold calibration, our work aims to mitigate such labor-intensive overhead by measuring metric K_s when no human is within the monitored area, and predicting a decision threshold without significant performance degradation.

8. Conclusion

In this paper, we harness PHY layer information available on commodity WiFi infrastructure to eliminate the on-site threshold calibration overhead involved in typical wireless passive human detection systems. On observing that the detection threshold relates to the link sensitivity level to human motions, which is a result of different multipath propagation conditions, we extract a quantitative metric from PHY layer CSI as an indicator for link sensitivity. We further exploit the metric to predict a threshold for human motion detection without on-site calibration. We prototype our model on commercial WiFi NICs and evaluate it in typical multipath-dense environments. Extensive experimental results show that the proposed threshold prediction model achieves comparative detection performance with the state-of-the-art. We envision this work as an early step towards calibration-free device-free environment and human sensing applications, which would facilitate fast and lightweight deployment of these systems in practical multipath-dense indoor environments.

Acknowledgment

This research is supported by the National Natural Science Foundation of China (Grant nos. 61170242, 61300206, 61472098 and 61572366), the Fundamental Research Funds for the Central Universities(Grant no. HEUCF100605) and NSF China under Grants no.61502520.

References

[1] L. Conceição, M. Curado, Onto scalable wireless ad hoc networks: adaptive and location-aware clustering, Ad Hoc Netw. 11 (8) (2013) 2484–2499.
[2] Z. Zhou, C. Wu, Z. Yang, Y. Liu, Sensorless Sensing with WiFi, ACM Comput. Surv. 20 (1) (2015) 1–6.
[3] M. Youssef, M. Mah, A. Agrawala, Challenges: device-free passive localization for wireless environments, in: Proceedings of ACM International Conference on Mobile Computing and Networking (MobiCom), 2007.
[4] M. Moussa, M. Youssef, Smart cevices for smart environments: device-free passive detection in real environments, in: Proceedings of the IEEE International Conference on Pervasive Computing and Communications, 2009. PerCom 2009., IEEE, 2009, pp. 1–6.
[5] A.E. Kosba, A. Saeed, M. Youssef, RASID: a robust WLAN device-free passive motion detection system, in: Proceedings of IEEE International Conference on Pervasive Computing and Communications (PerCom), 2012.
[6] Y. Zhao, N. Patwari, J.M. Phillips, S. Venkatasubramanian, Radio tomographic imaging and tracking of stationary and moving people via kernel distance, in: Proceedings of ACM International Conference on Information Processing in Sensor Networks (IPSN), 2013.
[7] J. Xiao, K. Wu, Y. Yi, L. Wang, L. Ni, FIMD: fine-grained device-free motion detection, in: Proceedings of IEEE International Conference on Parallel and Distributed Systems (ICPADS), 2012.
[8] J. Wilson, N. Patwari, A fade-level skew-laplace sgnal strength model for device-free localization with wireless networks, IEEE Trans. Mobile Comput. 11 (6) (2012) 947–958.
[9] N. Patwari, J. Wilson, Spatial models for human motion-induced signal strength variance on static links, IEEE Trans. Inf. Foren. Secur. 6 (3-1) (2011) 791–802.
[10] Y. Wen, X. Tian, X. Wang, S. Lu, Fundamental limits of rss fingerprinting based indoor localization, in: Proceedings of IEEE INFOCOM, 2015.
[11] D. Halperin, W. Hu, A. Sheth, D. Wetherall, Tool Release: gathering 802.11n traces with channel state information, ACM SIGCOMM Comput. Commun. Rev. 41 (1) (2011) 53.
[12] K. Qian, C. Wu, Z. Yang, Y. Liu, Z. Zhou, Pads: passive detection of moving targets with dynamic speed using phy layer information, in: Proceedings of IEEE ICPADS, 2014.
[13] W. Liu, X. Gao, L. Wang, D. Wang, Bfp: behavior-free passive motion detection using phy information, Wirel. Personal Commun. 83 (2) (2015) 1035–1055.
[14] J. Wilson, N. Patwari, See-through walls: motion tracking using variance-based radio tomography networks, IEEE Trans. Mobile Comput. 10 (5) (2011) 612–621.
[15] C. Xu, B. Firner, R.S. Moore, Y. Zhang, W. Trappe, R. Howard, F. Zhang, N. An, SCPL: indoor device-free multi-subject counting and localization using radio signal strength, in: Proceedings of ACM International Conference on Information Processing in Sensor Networks (IPSN), 2013.
[16] Y. Liu, Y. Zhao, L. Chen, J. Pei, J. Han, Mining frequent trajectory patterns for activity monitoring using radio frequency tag arrays, IEEE Trans. Parallel Distrib. Syst. 23 (11) (2012) 2138–2149.
[17] Z. Zhou, Z. Yang, C. Wu, L. Shangguan, Y. Liu, Omnidirectional coverage for device-free passive human detection, IEEE Trans. Parallel Distrib. Syst 25 (7) (2014) 1819–1829.
[18] S. Savazzi, M. Nicoli, F. Carminati, M. Riva, A Bayesian approach to device-free localization: modeling and experimental assessment, IEEE J. Select. Top. Signal Process. 8 (1) (2014) 16–29.
[19] O. Kaltiokallio, H. Yiğitler, R. Jäntti, A Three-State Received Signal Strength Model for Device-free Localization, arXiv preprint (2014).
[20] D. Zhang, Y. Liu, L.M. Ni, Link-centric probabilistic coverage model for transceiver-free object detection in wireless networks, in: Proceedings of IEEE International Conference on Distributed Computing Systems (ICDCS), 2010.
[21] Z. Yang, Z. Zhou, Y. Liu, From rssi to csi: indoor localization via channel response, ACM Comput. Surv. (CSUR) 46 (2) (2013) 25.
[22] K. Wu, J. Xiao, Y. Yi, M. Gao, L.M. Ni, FILA: fine-grained indoor localization, in: Proceedings of IEEE International Conference on Computer Communications (INFOCOM), 2012.
[23] J. Xiao, K. Wu, Y. Yi, L. Wang, L. Ni, Pilot: passive device-free indoor localization using channel state information, in: Proceedings of IEEE International Conference on Distributed Computing Systems (ICDCS), 2013.
[24] T. Rappaport, Wireless Communications: Principles and Practice, 2nd edition, Prentice Hall PTR, 2001.

[25] C. Tepedelenlioglu, A. Abdi, G. Giannakis, The Ricean K factor: estimation and performance analysis, IEEE Trans. Wirel. Commun. 2 (4) (2003) 799–810.
[26] F. Benedetto, G. Giunta, A. Toscano, L. Vegni, Dynamic LOS/NLOS statistical discrimination of wireless mobile channels, in: Proceedings of IEEE Vehicular Technology Conference (VTC), 2007.
[27] A. Sorrentino, G. Ferrara, M. Migliaccio, Kurtosis index to characterise near line-of-sight conditions in reverberating chambers, IET Microw., Antennas Propagat. 7 (3) (2013) 175–179.
[28] J. Zhang, M.H. Firooz, N. Patwari, S.K. Kasera, Advancing wireless link signatures for location distinction, in: Proceedings of ACM International Conference on Mobile Computing and Networking (MobiCom), 2008.
[29] S. Sen, B. Radunovic, R.R. Choudhury, T. Minka, You are facing the Mona Lisa: spot localization using PHY layer information, in: Proceedings of ACM International Conference on Mobile Systems, Applications, and Services (MobiSys), 2012.
[30] Z. Zhou, Z. Yang, C. Wu, W. Sun, Y. Liu, Lifi: line-of-sight identification with wifi, in: Proceedings of IEEE INFOCOM, 2014, pp. 2688–2696.
[31] A.A. Saleh, R.A. Valenzuela, A statistical model for indoor multipath propagation, IEEE J. Select. Areas Commun. 5 (2) (1987) 128–137.
[32] J. Wilson, N. Patwari, Radio tomographic imaging with wireless networks, IEEE Trans. Mobile Comput. 9 (5) (2010) 621–632.
[33] J. Han, C. Qian, P. Yang, D. Ma, Z. Jiang, W. Xi, J. Zhao, GenePrint: generic and accurate physical-layer identification for UHF RFID tag, IEEE/ACM Trans. Netw. (TON) (2015).

Liangyi Gong is currently a Ph.D. candidate in the Department of Computer Science and Technology, Harbin Engineering University. He received his B.E. degree in 2010 from the Department of Computer Science and Technology of Harbin Engineering University, Harbin, China. His main research interests include wireless networks and mobile computing.

Wu Yang received a Ph.D. degree in Computer System Architecture Specialty of Computer Science and Technology School from Harbin Institute of Technology. He is currently a professor and doctoral supervisor of Harbin Engineering University. His main research interests include wireless sensor network, peer-to-peer network and information security. He is a member of ACM and senior member of CCF.

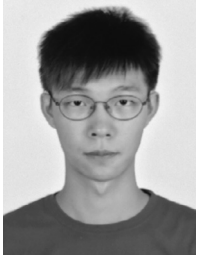

Zimu Zhou is currently a Ph.D. candidate in the Department of Computer Science and Engineering, Hong Kong University of Science and Technology. He received his B.E. degree in 2011 from the Department of Electronic Engineering of Tsinghua University, Beijing, China. His main research interests include wireless networks and mobile computing. He is a student member of IEEE and ACM.

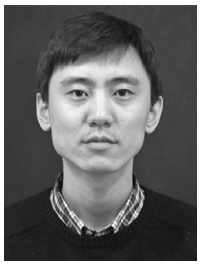

Dapeng Man received a Ph.D. degree in computer science and technology from Harbin Engineering University in 2009. He is currently an assistant professor in Harbin Engineering University. His main research interests include wireless sensor networks and mobile computing.

Haibin Cai is an associate professor in the Software Engineering Institute, East China Normal University. He received his Ph.D. degree from the Donghua University in 2008, Shanghai, China. He received his B.Eng. from the National University of Defense Technology in 1997, and M.S. degree from the National University of Defense Technology in 2004. His research interests include Internet of Things, Mobile Computing and Cyber-physical Systems.

Xiancun Zhou received the B.S. degree in electrical engineering from Anhui University, Hefei, China, in 1997, and received the M.S. degree in computer science from Heifei University of Technology, Heifei, China, in 2004. She is now a professor at the Department of Information Engineering in West Anhui University. Her current research interests include information security, and wireless networks.

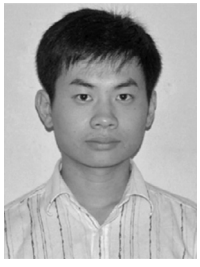

Zheng Yang received a B.E. degree in computer science from Tsinghua University in 2006 and a Ph.D. degree in computer science from Hong Kong University of Science and Technology in 2010. He is currently an assistant professor in Tsinghua University. His main research interests include wireless ad-hoc sensor networks and mobile computing. He is a member of the IEEE and the ACM.